JACS Au
AN OPEN ACCESS JOURNAL OF THE AMERICAN CHEMICAL SOCIETY

pubs.acs.org/jacsau
Article

Tailoring the Selective Oxidation of Hydroxyl-Containing Compounds via Precisely Tuning the Hydrogen-Bond Strength of Catalyst H-Bond Acceptors

Xiao Feng, Piaoping Yang, Yinwei Wang, Jieqi Cao, Jin Gao,* Song Shi,* and Dionisios G. Vlachos*

Cite This: JACS Au 2025, 5, 1359−1366
Read Online

ABSTRACT: The unique performance of the enzyme is mainly achieved via weak interactions between the "outer coordination sphere" and the substrate. Inspired by this process, we developed 3D encapsulated-structure catalysts with hydrogen-bond engineering on the shell, which mimics the "outer coordination sphere" of an enzyme. Various hydrogen bond acceptors (C═O, S═O, and N−O groups) are imparted in the shell. Concentration-dependent ^{1}H NMR, inverse-phase gas Chromatography (IGC) measurements, and DFT calculations underscore that the hydrogen bond strength between the acceptor groups and alcohol follows the order of C═O < S═O < N−O. The hydroxyl compound oxidation rate vs the hydrogen bond strength follows a volcano behavior, reminiscent of Sabatier's principle. The performance variation among catalysts is attributed to the adsorption strength of the substrate. The proposed bioinspired design principle expands the scope of encapsulated catalysts, enabling fine regulation of catalytic activity through precise microenvironment control via weak interactions with substrates.

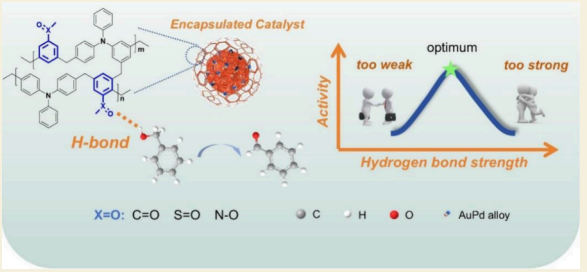

KEYWORDS: *enzyme-inspired, encapsulated catalyst, alcohol oxidation, hydrogen bond, Sabatier's principle*

INTRODUCTION

Enzymes are natural biocatalysts with high efficiency, selectivity, and specificity.[1] Artificial analogs mimicking enzyme catalysis have attracted great interest.[2] The unique structure of the protein scaffold structure is critical for enhancing performance, which comprises multiple coordination spheres, including the "active site" (the metal center and the first and second coordination spheres) and the "outer coordination sphere" (the remaining protein scaffold).[3] Despite its distance from the active site, it plays a significant role in catalytic reactions.[4−6] Shaw's pioneering work on electrocatalytic hydrogen production and oxidation has demonstrated that the outer coordination sphere exerts a significant influence on rate and overpotential, affecting proton movement and structure.[4,7] Cargnello et al. designed a three-dimensional nanocatalyst (POF/Pd/POF) in which Pd nanocrystals were encapsulated within microporous organic frameworks (POFs), impacting the transition state of CO oxidation and the transport of CO_2.[8]

Enzymes' performance depends on the substrate-binding pocket interactions, including hydrophobic interactions, electrostatic attractions, and disulfide bonds.[5,9] Among them, the hydrogen bond is the most common. To emulate hydrogen bonding, we introduced interactions between the substrate C═O groups and the catalyst's proton donors (OH groups). Selective hydrogenation of C═O groups was promoted due to the enhanced adsorption of an aldehyde via hydrogen bonds.[10]

Apart from typical hydrogen bonds, the hydrogen bond strength is important.[11,12] For example, short, strong hydrogen bonds (SSHBs) at the active site of several enzymes exist with a proton donor−acceptor distance of less than 2.7 Å.[13] In the hydroxynitrile lyase from Hevea brasiliensis (HbHNL), a short hydrogen bond between the two residues of the catalytic triad (2.67 Å between Nσ(His^{235}) and Oε(Asp^{207})) forms when the competitive inhibitor thiocyanate combines with the HbHNL.[12] Up to now, there have been challenges in regulating the strength of the hydrogen-bond interaction and the subsequent catalytic activity.

The hydroxyl group (−OH) is one of the essential functional groups in the biobased building blocks, and its transformation has attracted a lot of attention.[14] However, hydroxyl groups are capable of forming hydrogen bonds (intermolecular hydrogen bonds or hydrogen bonds with the solvent molecule), which brings a barrier to their efficient conversion.[15] Some exploratory works try to resolve it by forming stronger hydrogen bonds with deep eutectic solvents

Received: December 23, 2024
Revised: February 4, 2025
Accepted: February 7, 2025
Published: February 20, 2025

https://doi.org/10.1021/jacsau.4c01262
JACS Au 2025, 5, 1359−1366

(DESs) or ionic liquid, which not only breaks the original hydrogen bond but also activates the hydroxyl group through decreasing electron cloud density.[16,17] In our previous work,[18] we have shown that the hydrogen bond is able to enhance the oxidation rate; however, the effect of the hydrogen bond strength remains to be investigated.

Recently, the effect of hydrogen bonds on chemical reactions has attracted attention.[19−21] Currently, research work compares systems with or without hydrogen bonds.[22] It is difficult to precisely tune and understand the role of the hydrogen bond strength in a reaction. Wang et al.[20] revealed that the hydrogen bond strength between oxygen-reduction reaction (ORR) products and ionic liquids could influence the intrinsic ORR activity. Gomes et al.[19] found that the hydrogen bond network could modulate the hydrogen evolution reaction (HER) activity and carbon dioxide reduction (CO_2R) selectivity, via tuning the water solvation and dynamics of aprotic solvents featuring different donor abilities.

Here, we synthesize 3D encapsulation catalysts with an outer shell that does not affect the AuPd active sites. We introduce different hydrogen acceptors into the outer shell to tune the strength of the hydrogen bond interactions with an alcohol (Scheme 1). The hydrogen bond strength was quantified by

Scheme 1. Schematic Diagram for the Synthesis of the Encapsulated Catalysts

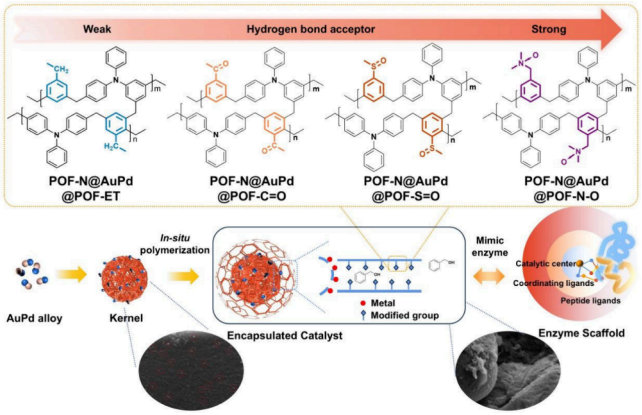

concentration-dependent ^{1}H NMR and IGC. The oxidation rate vs the hydrogen bond strength exhibited a volcano curve. This work reveals that the catalytic performance is mainly controlled by the adsorption of the substrate, captured by Sabatier's principle.

RESULTS AND DISCUSSION

Catalyst Preparation and Characterization

Encapsulating structure catalysts were designed to distinguish the catalytic site from microenvironment effects. AuPd alloy nanoparticles with a diameter of 3−6 nm (Figure S1), presynthesized using the sol-immobilization method,[23] were supported on the same kernel (triphenylamine polymer, labeled as POF-N) and encapsulated by shells of various hydrogen acceptor groups (POF-N@AuPd@POF-X, X = S═O group, C═O group, N−O group). For comparison, we also synthesized a catalyst without hydrogen acceptor groups (ethyl group) labeled as POF-N@AuPd@POF-ET (Scheme 1).

The interplanar spacing in a typical lattice fringe of individual AuPd/POF-N particles was 0.233 nm (Figure 1a, detailed lattice spacing measurement in Figure S2), right between Au (111) (0.236 nm) and Pd (111) (0.224 nm), further confirming a AuPd alloy.[24,25] Figure 1b−d shows TEM images of the pure AuPd NPs, AuPd NPs supported on inner kernel POF-N, and AuPd NPs in an encapsulated catalyst, respectively. TEM images of AuPd/POF-N reveal homogeneously dispersed particles in the kernel (Figure 1c). As shown in Figure 1e, the diffraction patterns of AuPd alloys on the kernel AuPd/POF-N show four diffraction rings, corresponding to (111), (200), (220), and (311) planes of AuPd nanoparticles, suggesting the AuPd is polycrystalline bimetallic NPs.[26] Figure 1f shows an STEM image of a typical core AuPd/POF-N. The similar distribution of Au and Pd in the elemental mapping suggests an alloy structure, consistent with XRD and XPS data.[25,27] In addition, similar signals imply that the alloy maintained its original state after encapsulation (Figures S3−S4).

HR-TEM, *in situ* ion sputtering XPS, and FE-SEM were used to verify the encapsulated structure. TEM showed a decreased contrast of AuPd NPs in POF-N@AuPd@POF-C═O (Figure 1d) due to kernel encapsulation (AuPd/POF-N) within the POFs.[8,28] Compared to the kernel AuPd/POF-N ((i), Figure 1g) the Au 4f signal of the encapsulated catalyst almost disappeared (ii) due to the kernel masking by the outer polymer. The lack of signal stems from the maximum penetration depth of XPS (the encapsulation of the outer layer polymer on the kernel was at least 5 nm). Upon removing part of the outer layer by XPS ion sputtering, the inner metal particles partially exposed the Au 4f signal (iii in Figure 1g).[8] POF-N@AuPd@POF-C═O showed a similar enhancement in the Au 4f signal to POF-N@AuPd@POF-N-O by *in situ* argon ion sputtering as shown in Figure S5. According to the FE-SEM images (Figure S6), metal nanoparticles could be observed on the kernel but not on the encapsulated catalyst surface.

The hydrogen bond acceptor groups on the exterior polymer were characterized using ss-^{13}C NMR. All samples exhibited nuclear magnetic peaks at 141 and 128 ppm due to substituted and unsubstituted aromatic carbon, respectively. Aromatic monomers with various functional groups displayed distinct differences in the high field (Figure 1h). The signal at 14 ppm on the POF-ET corresponds to the carbon of the methyl group and that at 25 ppm to the benzyl carbon. The peak at 19 ppm in POF-C═O is assigned to the methyl group, and the 193 ppm matches the carbon of the carbonyl group. For POF-S═O, the signal at 57 ppm was attributed to the carbon of the methyl group due to the strong electron-withdrawing effect of the sulfoxide group.[29] For POF-N-O, peaks at 49 and 57 ppm matched the carbon of the methyl and benzyl groups near the N−O group, respectively.

FT-IR spectroscopy identified the functional groups in the polymer shells. Compared with the polymer POF-ET, the sulfoxide group showed a characteristic peak at 1039 cm^{-1} and the carbonyl group at 1680 cm^{-1}. In POF-N-O, the characteristic peak of the N−O group is at 1350 cm^{-1} (Figure S7).[30]

In addition, according to N_2 adsorption−desorption analysis at 77 K (Figure S8), all encapsulated catalysts showed large surface areas and abundant pores, enabling the substrate to reach the active sites. Importantly, these polymers remain stable up to 300 °C in air (Figure S9), suggesting thermal stability at the reaction temperature. These findings, taken

https://doi.org/10.1021/jacsau.4c01262
JACS Au 2025, 5, 1359−1366

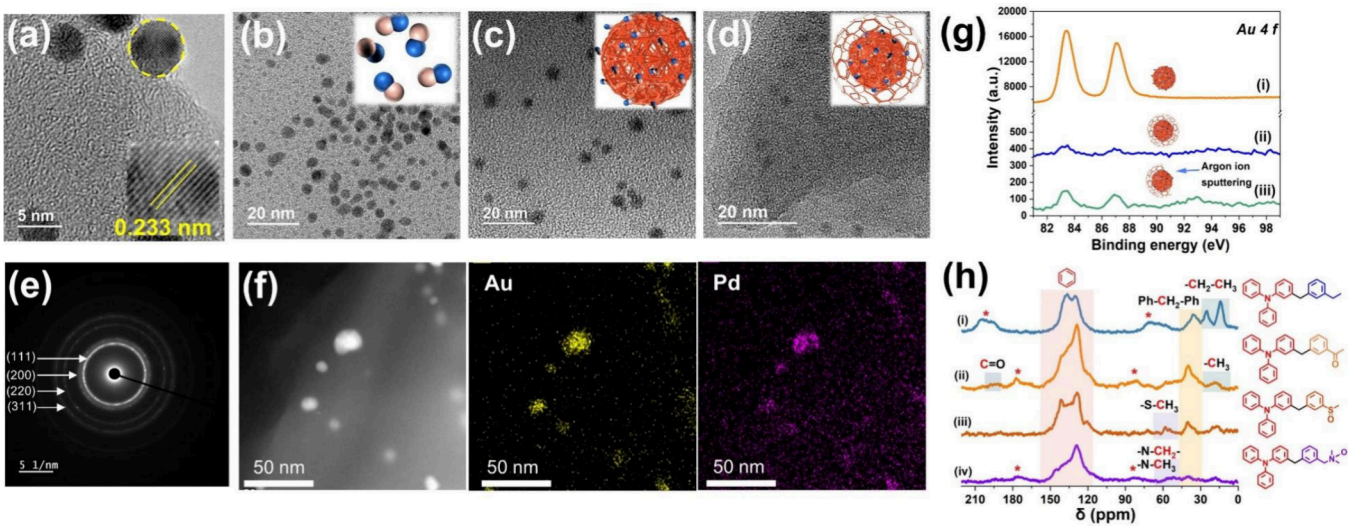

Figure 1. a. HR-TEM image of AuPd/POF-N and corresponding lattice spacing; b–d. TEM images of (b) AuPd NPs; (c) AuPd NPs supported on inner kernel POF-N; and (d) AuPd NPs encapsulated in POF-N@AuPd@POF-C═O. e. Selected area electron diffraction (SAED) patterns of AuPd/POF-N. f. HAADF-STEM image of AuPd/POF-N and corresponding elemental mapping of Au and Pd of AuPd/POF-N. g. XPS spectra of (i) AuPd/POF-N, (ii) POF-N@AuPd@POF-N-O, and (iii) *in situ* argon ion sputtering on the shell of catalyst POF-N@AuPd@POF–N-O. h. Solid-state ^{13}C CP/MAS NMR spectra of polymers POF-X (X = ET group, C═O group, S═O group, and N–O group); the asterisks denote spinning sidebands. (i) POF-ET, (ii) POF-C═O, (iii) POF-S═O, and (iv) POF-N-O.

together, demonstrate the successful synthesis of outer layer polymers with similar structures and diverse compositions.

Catalyst Performance in Oxidation of Alcohols

The aerobic oxidation of benzyl alcohol to benzaldehyde was chosen as a model reaction to investigate the effect of hydrogen bonding. With the same content of active site AuPd alloys (Table S1), POF-N@AuPd@POF-ET, POF-N@AuPd@POF-N-O, POF-N@AuPd@POF-C═O, and POF-N@AuPd@POF-S═O catalysts with similar aromatic structures exhibit distinct TOFs of 28, 30, 36, and 45 h^{-1} (Figure 2, Table S2), respectively. Catalysts containing hydrogen-bond acceptor groups are more active than the POF-N@AuPd@POF-ET (Figures S10–S11).

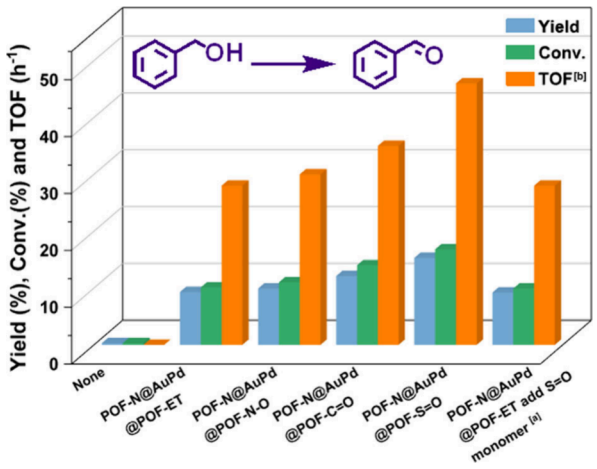

Figure 2. Catalytic oxidation of benzyl alcohol over various catalysts. Reaction conditions: 120 °C, 1.0 MPa initial O_2, 10 mL of CH_3CN, 1.0 mmol substrate, 50 mg catalyst, 4 h. Note: [a] POF-N@AuPd@POF-ET with 49 mg methyl phenyl sulfoxide monomer. [b] TOF measured based on the initial oxidation rate with the conversion at about 10% using the total amount of AuPd metal sites.

The catalysts can be reused for at least three cycles (Figure S12). The FT-IR spectra and TEM images of Figures S13 and S14 demonstrate the structural stability of the spent encapsulated catalysts.

To verify the active site of the encapsulated catalysts, we compared the oxidation of the monometallic supported catalysts, physically mixed monometallic catalysts (Au/POF-N + Pd/POF-N), and the AuPd alloy catalyst. The AuPd alloy catalyst showed enhanced alcohol oxidation, indicating that the AuPd alloy is catalytically active (Figure S15). Compared with supported catalysts, encapsulated catalysts with hydrogen-bond-accepting functionalities are superior (Table S3).

Interestingly, when the hydrogen-bond acceptor monomer was physically mixed with POF-N@AuPd@POF-ET, little promotion was seen, illustrating the importance of surface intimacy in Figure 2. We postulate that the enhanced catalytic performance stems from the hydrogen bond acceptor groups on the catalyst that interact with the substrate alcohol.

Hydrogen Bond Interactions

Substrate concentration-dependent ^1H NMR tests provide insights into the hydrogen bond strength. The chemical shift of H in the –OH group of benzyl alcohol remained at 1.6 ppm as the concentration of ethylbenzene increased in CD_3Cl (Figure 3a), indicating no hydrogen bond formation. While in a particular concentration range (ratio at 1.6), the chemical shift of the –OH proton moves from 1.6 to 9.43 ppm with the proton acceptor N–O group of the *N*-dimethylbenzylamine-nitrogen oxide (Figure 3d). Similarly, as the S═O group from methyl phenyl sulfoxide and the C═O group from acetophenone increased, the chemical shift of the OH proton moved downfield from 1.6 to 2.06 and 1.74 ppm, respectively (Figure 3b,c). These shifts reflect that the proton-acceptor ability of the functional groups decreases in the order of N–O > S═O > C═O > Et. The corresponding Gibbs free energy change (ΔG) was calculated from the hydroxyl proton chemical shift ($\Delta\delta$) changes with the concentration (C) variation:[17,31]

https://doi.org/10.1021/jacsau.4c01262
JACS Au 2025, 5, 1359–1366

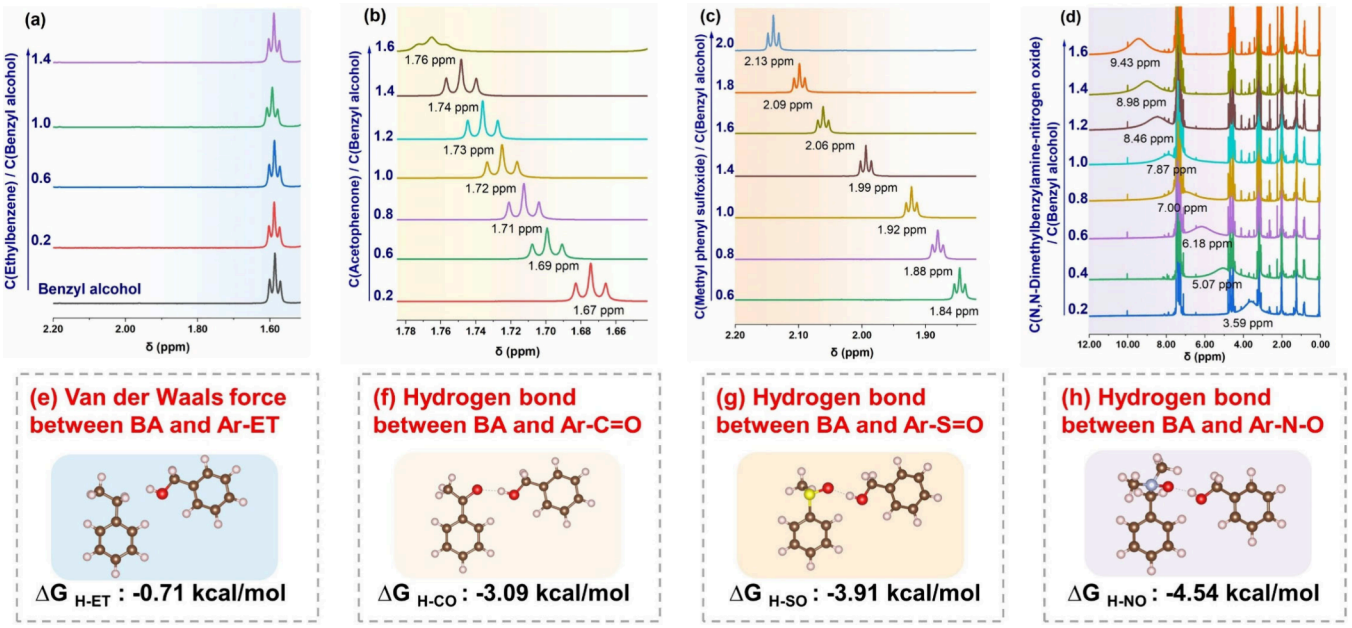

Figure 3. a–d. Characterization of hydrogen bond interactions using concentration-variation ^{1}H NMR spectra. (a) Ethylbenzene/benzyl alcohol, (b) acetophenone/benzyl alcohol, (c) methyl phenyl sulfoxide/benzyl alcohol, and (d) nitrogen dimethylbenzylamine-nitrogen oxide/benzyl alcohol in $CDCl_3$ at different concentration ratios. Note: concentration-dependent ^{1}H NMR tests were performed by varying the concentrations of hydrogen bond acceptors and retaining the concentration of proton donor benzyl alcohol in the initial hydrogen bond system. e–h. Optimized configuration and interaction of benzyl alcohol (BA) with (e) ethylbenzene (Ar-ET), (f) acetophenone (Ar–C═O), (g) methyl phenyl sulfoxide (Ar–S═O), and (h) nitrogen dimethylbenzylamine-nitrogen oxide (Ar–N–O) from DFT calculations.

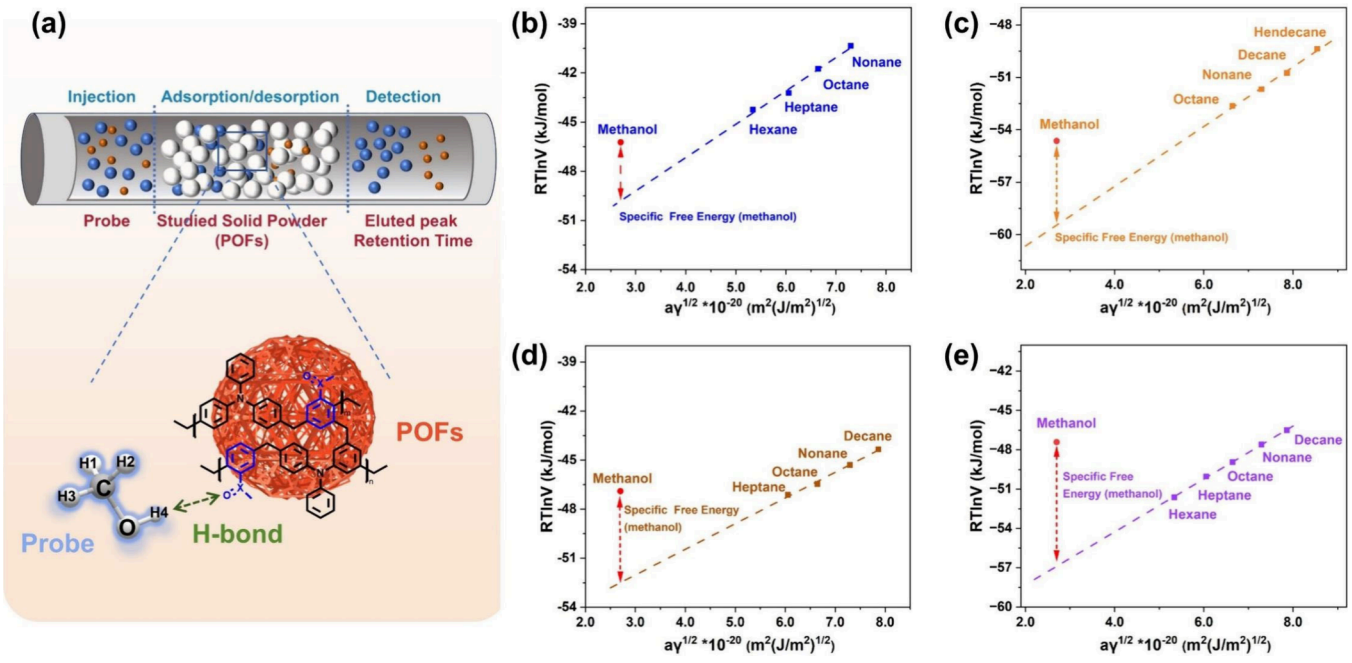

Figure 4. a. Schematic depiction of the IGC setup. b–e. IGC plots of different POFs: (b) POF-ET, (c) POF-C═O, (d) POF-S═O, (e) POF-N-O. The gap value represents the specific free energy ($\Delta G^{Sp}_{methanol}$), calculated from the deviation of calculated $RT \ln V$ values of methanol from the gradient of the plot of $RT \ln V$ versus $a\gamma^{1/2}$ obtained from dispersion forces from nonpolar adsorbates.

$$\Delta G = RT \ln(K) \quad (1)$$

$$1/\Delta\delta = a \times 1/K \times 1/C + a \quad (2)$$

The hydrogen bond energies for ΔG_{H-CO}, ΔG_{H-SO}, and ΔG_{H-NO} are −0.23 kcal/mol, −0.55 kcal/mol, and −1.68 kcal/mol, respectively (Table S7) (for further details, see Figures S16–S18, Tables S4–S6).

Similarly, the chemical shift of the OH proton moved downfield as the concentration of the proton acceptor increased in CD_3CN, which serves as the reaction solvent (Figures S19–S20). The shifts indicate the hydrogen bond strength also decreases in the order of N–O > S═O > C═O under the reaction medium.

https://doi.org/10.1021/jacsau.4c01262
JACS Au 2025, 5, 1359–1366

DFT calculations were conducted to investigate the hydrogen bond interaction between the hydrogen bond donor (H of the OH group in benzyl alcohol) and various hydrogen bond acceptors. Considering that POFs are amorphous and difficult to model, we chose four molecules containing the ethyl group, C═O group, S═O group, and N−O group to simplify the computational models (Figure 3e−h). The interaction between the ethyl group and H of the OH group in benzyl alcohol, mainly via van der Waals interactions, is weak (−0.71 kcal/mol). Hydrogen bonds enhance the interaction strength. Specifically, the calculated hydrogen bond energies for the C═O group (ΔG_{H-CO}), S═O group (ΔG_{H-SO}), and N−O group (ΔG_{H-NO}) are −3.09 kcal/mol, −3.91 kcal/mol, and −4.54 kcal/mol, respectively, following the order of N−O > S═O > C═O, consistent with the experimental results. Moreover, the hydrogen bond length for the C═O group (2.14 Å), S═O group (1.99 Å), and N−O group (1.95 Å) exhibits a reverse order.

Hydrogen bond energy calculations (Figure S21, Table S8) using molecules with more aromatic rings, more closely representing actual polymers, show that the hydrogen bond energies increase and that the order of N−O > S═O > C═O remains. Importantly, the gap between ΔG_{H-CO} and ΔG_{H-NO} is generally consistent, and that of ΔG_{H-SO} and ΔG_{H-NO} shows a similar trend (Figure S22). These results suggest that the hydrogen bond strength order of N−O > S═O > C═O would still hold in actual catalysts.

To further assess the hydrogen bond between the substrate and catalyst surface, inverse-phase gas chromatography (IGC) experiments were performed. IGC is effective in evaluating the polar surface free energy of a material quantitatively.[32,33] The higher the polar surface free energy is, the stronger the material's affinity toward polar molecules.[33] Methanol, which contains OH groups, was selected as the probe molecule. The special free energies of methanol adsorption ($\Delta G^{Sp}_{methanol}$) were determined to be −2.26, −1.33, −1.10, and −0.84 kcal/mol, for the polymers with N−O, S═O, C═O, and Et groups, respectively (Figure 4 (for further details see Tables S9−S10).

The hydrogen bond free energy from ^{1}H NMR tests and IGC tests correlates linearly with Figure S23, revealing that the affinity difference of the alcohol substrate stems from the varying hydrogen bonding.

According to IGA (intelligent gravimetric analyzer) experiments, the hydrogen bond interaction affects the adsorption capacity. Polymers with hydrogen bond acceptor groups display higher adsorption capacity toward methanol than POF-ET (Figure S24). Under the premise of the same AuPd/POF-N core, we characterized the properties of the shell polymers by IGC and IGA to reveal the influence of different hydrogen bond acceptors on the shell polymer of the encapsulated catalyst directly.

The adsorption isotherms of benzyl alcohol on encapsulated catalysts are shown in Figure S25. The uptake of benzyl alcohol capacity follows the order: POF-N@AuPd@POF-N-O > POF-N@AuPd@POF-S═O > POF-N@AuPd@POF-C═O > POF-N@AuPd@POF-ET, probably due to the different affinity of the alcohol to the shell caused by the different hydrogen bonding strength.

The TOF vs the strength of hydrogen bonds from ^{1}H NMR displays a volcano (Figure 5). It increases initially with increasing hydrogen bond strength but decreases when the strength is too high (for the N−O group). According to DFT calculations, the volcano trend vs the hydrogen bond strength

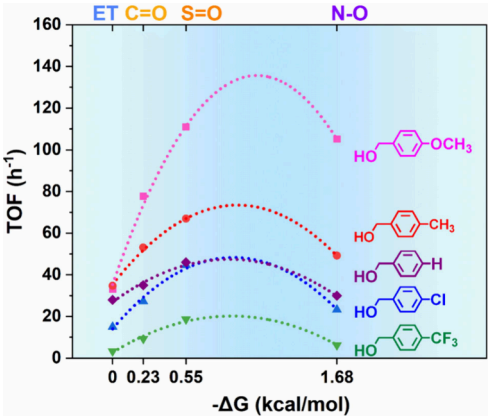

Figure 5. Experimentally estimated TOF of aromatic alcohol catalytic oxidation on encapsulated catalysts vs hydrogen bond energy from ^{1}H NMR quantification. Dotted lines are an interpolation of the experimental data (points).

is retained as the number of aromatic rings increases (Figure S26). The maximum rate occurs for a hydrogen bond acceptor close to the S═O group.

Several experiments were conducted to clarify the mechanistic differences. The reaction rate (Figure S27) was of a pseudozero order with respect to O_2. The reaction order of benzyl alcohol (Figure S28) was first order. This data clearly showed that the rate enhancement was benzyl alcohol related instead of O_2, further confirming the importance of the hydrogen bond. The catalysts showed negative ρ values in the Hammett plots (Figure S29), indicating that all reactions had positive charge accumulation on the benzylic carbon.[34] Kinetic isotope effect (KIE) experiments suggested that the αC−H cleavage is the rate-determining step on all catalysts (Table S11, Figure S30).[34] Considering the consistency of the active site and the above evidence, we deduce that the benzyl alcohol oxidation evolves by the same mechanism for all catalysts.

Given the same active site and reaction route, the enhanced catalytic activity is then attributed to the substrate adsorption strength modulated by hydrogen bonding. Based on Sabatier's principle, a suitable substrate adsorption strength on an active center/catalyst is needed.[35] Weak interactions lead to a low substrate population and strong binding to overcrowding and a slow turnover. Moderate hydrogen bonding is most effective for oxidation. Since Sabatier's principle is common in enzyme catalysis, our work brings further parallels of heterogeneous and enzyme catalysis.

CONCLUSION

This work encapsulated AuPd alloy nanoparticles with polymers of various hydrogen bond acceptor groups (N−O, C═O, and S═O). Concentration-dependent ^{1}H NMR, IGC, and IGA experiments and DFT calculations revealed hydrogen bonds between the hydrogen bond acceptor and benzyl alcohol with the strength varying as C═O < S═O < N−O. Under the premise of excluding other factors as far as possible, the catalytic performance is predominantly influenced by hydrogen bonding. The hydrogen bond primarily modulates the adsorption of the substrate and results in a volcano reaction rate: moderate hydrogen bonding favors the reaction, consistent with Sabatier's principle.

This work realizes that fine-tuning weak interactions (hydrogen bond interactions) toward substrates on heteroge-

https://doi.org/10.1021/jacsau.4c01262
JACS Au 2025, 5, 1359−1366

neous catalysts, which emulate enzyme catalysts, provides an approach to improving them.

■ ASSOCIATED CONTENT

Supporting Information

The Supporting Information is available free of charge at https://pubs.acs.org/doi/10.1021/jacsau.4c01262.

Additional experimental details, materials, and methods, including DFT calculations, catalytic performance, XPS and XRD patterns spectra, N_2 adsorption−desorption isotherms, pore size distributions, TEM and FE-SEM images, FT-IR, Thermogravimetric analysis, IGC and IGA results, NMR spectra, Hammett studies and adsorption isotherms results and supplementary tables and reference (PDF)

■ AUTHOR INFORMATION

Corresponding Authors

Jin Gao − *State Key Laboratory of Catalysis, Dalian Institute of Chemical Physics, Chinese Academy of Sciences, Dalian 116023, China*; Email: gaojin@dicp.ac.cn

Song Shi − *State Key Laboratory of Catalysis, Dalian Institute of Chemical Physics, Chinese Academy of Sciences, Dalian 116023, China*; orcid.org/0000-0002-4306-1933; Email: shisong@dicp.ac.cn

Dionisios G. Vlachos − *Department of Chemical and Biomolecular Engineering and Catalysis Center for Energy Innovation (CCEI), University of Delaware, Newark, Delaware 19716, United States*; orcid.org/0000-0002-6795-8403; Email: vlachos@udel.edu

Authors

Xiao Feng − *State Key Laboratory of Catalysis, Dalian Institute of Chemical Physics, Chinese Academy of Sciences, Dalian 116023, China; University of Chinese Academy of Sciences, Beijing 100049, China*

Piaoping Yang − *Department of Chemical and Biomolecular Engineering and Catalysis Center for Energy Innovation (CCEI), University of Delaware, Newark, Delaware 19716, United States*

Yinwei Wang − *State Key Laboratory of Catalysis, Dalian Institute of Chemical Physics, Chinese Academy of Sciences, Dalian 116023, China; University of Chinese Academy of Sciences, Beijing 100049, China*

Jieqi Cao − *State Key Laboratory of Catalysis, Dalian Institute of Chemical Physics, Chinese Academy of Sciences, Dalian 116023, China; University of Chinese Academy of Sciences, Beijing 100049, China*

Complete contact information is available at: https://pubs.acs.org/10.1021/jacsau.4c01262

Author Contributions

X.F. performed the preparation and characterizations of catalysts, catalyst effect tests, and manuscript writing. P.Y. contributed to the DFT calculations. Y.W. carried out the HR-TEM tests. J.C. participated in the catalyst preparation and product analysis. J.G. and P.Y. discussed the results and assisted with the manuscript preparation. S.S. and D.G.V. designed the project and revised the manuscript. All authors reviewed and commented on the manuscript. CRediT: **Xiao Feng** data curation, formal analysis, investigation, methodology, writing - original draft, writing - review & editing; **Piaoping Yang** formal analysis, software, writing - review & editing; **Yinwei Wang** writing - review & editing; **Jieqi Cao** writing - review & editing; **Jin Gao** supervision; **Song Shi** conceptualization, funding acquisition, project administration, supervision, writing - review & editing; **Dionisios G. Vlachos** conceptualization, funding acquisition, supervision, writing - review & editing.

Notes

The authors declare no competing financial interest.

■ ACKNOWLEDGMENTS

This work was supported in part by the following funds: National Key Research and Development Program of China (2022YFA1504900), the National Natural Science Foundation of China (Grant nos. 22072147, 22372168), and the Youth Innovation Promotion Association, the Chinese Academy of Sciences (2021178). P.Y. and D.G.V.'s work was supported by the Catalysis Center for Energy Innovation, an Energy Frontier Research Center funded by the US Dept. of Energy, Office of Science, Office of Basic Energy Sciences, under award number DE-SC0001004, and we greatly thank Prof. Jie Xu for the helpful conversations.

■ REFERENCES

(1) (a) Benkovic, S. J.; Hammes-Schiffer, S. A perspective on enzyme catalysis. *Science* **2003**, *301*, 1196−1202. (b) Punekar, N. *Enzymes: catalysis, kinetics and mechanisms*; Springer, 2018.

(2) Saha, R.; Mondal, B.; Mukherjee, P. S. Molecular cavity for catalysis and formation of metal nanoparticles for use in catalysis. *Chem. Rev.* **2022**, *122*, 12244−12307.

(3) Ginovska, B.; Gutiérrez, O. Y.; Karkamkar, A.; Lee, M.-S.; Lercher, J. A.; Liu, Y.; Raugei, S.; Rousseau, R.; Shaw, W. J. Bioinspired Catalyst Design Principles: Progress in Emulating Properties of Enzymes in Synthetic Catalysts. *ACS Catal.* **2023**, *13*, 11883−11901.

(4) Darmon, J. M.; Kumar, N.; Hulley, E. B.; Weiss, C. J.; Raugei, S.; Bullock, R. M.; Helm, M. L. Increasing the rate of hydrogen oxidation without increasing the overpotential: a bio-inspired iron molecular electrocatalyst with an outer coordination sphere proton relay. *Chem. Sci.* **2015**, *6*, 2737−2745.

(5) Kuah, E.; Toh, S.; Yee, J.; Ma, Q.; Gao, Z. Enzyme Mimics: Advances and Applications. *Chemistry* **2016**, *22*, 8404−8430.

(6) Yang, X.; Xu, Q. Encapsulating Metal Nanocatalysts within Porous Organic Hosts. *Trends in Chemistry* **2020**, *2*, 214−226.

(7) Ginovska-Pangovska, B.; Dutta, A.; Reback, M. L.; Linehan, J. C.; Shaw, W. J. Beyond the active site: the impact of the outer coordination sphere on electrocatalysts for hydrogen production and oxidation. *Acc. Chem. Res.* **2014**, *47*, 2621−2630.

(8) Riscoe, A. R.; Wrasman, C. J.; Herzing, A. A.; Hoffman, A. S.; Menon, A.; Boubnov, A.; Vargas, M.; Bare, S. R.; Cargnello, M. Transition state and product diffusion control by polymer−nanocrystal hybrid catalysts. *Nat. Catal.* **2019**, *2*, 852−863.

(9) (a) Coulther, T. A.; Ko, J.; Ondrechen, M. J. Amino acid interactions that facilitate enzyme catalysis. *J. Chem. Phys.* **2021**, *154*, No. 195101. (b) Mazmanian, K.; Sargsyan, K.; Lim, C. How the Local Environment of Functional Sites Regulates Protein Function. *J. Am. Chem. Soc.* **2020**, *142*, 9861−9871. (c) Knowles, R. R.; Jacobsen, E. N. Attractive noncovalent interactions in asymmetric catalysis: links between enzymes and small molecule catalysts. *Proc. Natl. Acad. Sci. U. S. A.* **2010**, *107*, 20678−20685. (d) Benkovic, S. J.; Hammes-Schiffer, S. A Perspective on Enzyme Catalysis. *Science* **2003**, *301*, 1196−1202.

(10) Shi, S.; Yang, P.; Dun, C.; Zheng, W.; Urban, J. J.; Vlachos, D. G. Selective hydrogenation via precise hydrogen bond interactions on catalytic scaffolds. *Nat. Commun.* **2023**, *14*, 429.

(11) (a) Hubbard, R. E.; Kamran Haider, M. Hydrogen Bonds in Proteins: Role and Strength. *eLS* **2010**, DOI: 10.1002/9780470015902.a0003011.pub2. (b) Kumar, M.; Balaji, P. V. C-H···pi interactions in proteins: prevalence, pattern of occurrence, residue propensities, location, and contribution to protein stability. *J. Mol. Model.* **2014**, *20*, 2136. (c) Oksanen, E.; Chen, J. C.-H.; Fisher, S. Z. Neutron crystallography for the study of hydrogen bonds in macromolecules. *Molecules* **2017**, *22*, 596.
(12) Derewenda, Z. S.; Lee, L.; Derewenda, U. The occurrence of C-H···O hydrogen bonds in proteins. *J. Mol. Biol.* **1995**, *252*, 248−262.
(13) Rajagopal, S.; Vishveshwara, S. Short hydrogen bonds in proteins. *FEBS J.* **2005**, *272*, 1819−1832.
(14) (a) van Putten, R.-J.; van der Waal, J. C.; de Jong, E.; Rasrendra, C. B.; Heeres, H. J.; de Vries, J. G. Hydroxymethylfurfural, A Versatile Platform Chemical Made from Renewable Resources. *Chem. Rev.* **2013**, *113*, 1499−1597. (b) Qu, R.; Junge, K.; Beller, M. Hydrogenation of Carboxylic Acids, Esters, and Related Compounds over Heterogeneous Catalysts: A Step toward Sustainable and Carbon-Neutral Processes. *Chem. Rev.* **2023**, *123*, 1103−1165. (c) Shalumova, T.; Tanski, J. M. 5-(Hydroxymethyl)furan-2-carbaldehyde. *Acta Crystallogr., Sect. E: Struct. Rep. Online* **2010**, *66*, o2266−o2266.
(15) (a) Kuhn, L. P. The Hydrogen Bond. I. Intra-and Intermolecular Hydrogen Bonds in Alcohols1. *J. Am. Chem. Soc.* **1952**, *74*, 2492−2499. (b) Fox, J. J.; Martin, A. E. Infra-red absorption of the hydroxyl group in relation to inter- and intramolecular hydrogen bonds. *Trans. Faraday Soc.* **1940**, *36*, 897. (c) Guchhait, N.; Ebata, T.; Mikami, N. Structures of hydrogen-bonded clusters of benzyl alcohol with water investigated by infrared-ultraviolet double resonance spectroscopy in supersonic jet. *J. Chem. Phys.* **1999**, *111*, 8438−8447. (d) Maréchal, Y. *The hydrogen bond and the water molecule: The physics and chemistry of water, aqueous and bio-media*; Elsevier, 2006.
(16) (a) Chu, F.; Lu, B.; Zhao, G.; Zhu, Z.; Yang, K.; Su, T.; Zhang, Q.; Chen, C.; Lü, H. Aerobic Oxidation of 5-Hydroxymethylfurfural via Hydrogen Bonds Reconstruction with Ternary Deep Eutectic Solvents. *ChemSusChem* **2024**, *17*, No. e202301385. (b) Nguyen, H. V. D.; De Vries, R.; Stoyanov, S. D. Natural Deep Eutectics as a "Green" Cellulose Cosolvent. *ACS Sustainable Chem. Eng.* **2020**, *8*, 14166−14178. (c) Chundawat, S. P. S.; Bellesia, G.; Uppugundla, N.; da Costa Sousa, L.; Gao, D.; Cheh, A. M.; Agarwal, U. P.; Bianchetti, C. M.; Phillips, G. N.; Langan, P.; et al. Restructuring the Crystalline Cellulose Hydrogen Bond Network Enhances Its Depolymerization Rate. *J. Am. Chem. Soc.* **2011**, *133*, 11163−11174.
(17) Luo, Y.; Ma, H.; Zhang, S.; Zheng, D.; Che, P.; Liu, X.; Zhang, M.; Gao, J.; Xu, J. Binding Energy as Driving Force for Controllable Reconstruction of Hydrogen Bonds with Molecular Scissors. *J. Am. Chem. Soc.* **2020**, *142*, 6085−6092.
(18) Feng, X.; Shi, S.; Zhu, G.; Wang, Y.; Cao, J.; Xu, J. Surface-Modified S = O Microenvironment Boosts Catalyzed Oxidation of Alcohol via Hydrogen Bond Interactions. *ACS Catal.* **2024**, *14*, 776−784.
(19) Gomes, R. J.; Kumar, R.; Fejzić, H.; Sarkar, B.; Roy, I.; Amanchukwu, C. V. Modulating water hydrogen bonding within a non-aqueous environment controls its reactivity in electrochemical transformations. *Nat. Catal.* **2024**, *7*, 689−701.
(20) Wang, T.; Zhang, Y.; Huang, B.; Cai, B.; Rao, R. R.; Giordano, L.; Sun, S.-G.; Shao-Horn, Y. Enhancing oxygen reduction electrocatalysis by tuning interfacial hydrogen bonds. *Nat. Catal.* **2021**, *4*, 753−762.
(21) Zhang, J.; Zeng, H.; He, B.; Liu, Y.; Xu, J.; Niu, T.; Pan, C.; Zhang, Y.; Lou, Y.; Wang, Y.; et al. Suppressing the hydrogen bonding interaction with *OOH toward efficient H2O2 electrosynthesis via remote electronic tuning of Co-N4. *Applied Catalysis B: Environment and Energy* **2024**, *358*, No. 124448.
(22) (a) Zhou, W.; Lai, R.; Cheng, Y.; Bao, Y.; Miao, W.; Cao, X.; Jia, G.; Li, G.; Li, C. Insights into How NH4+ Ions Enhance the Activity of Dimeric G-Quadruplex/Hemin DNAzyme. *ACS Catal.* **2023**, *13*, 4330−4338. (b) Ma, X.; Shi, Y.; Liu, J.; Li, X.; Cui, X.; Tan, S.; Zhao, J.; Wang, B. Hydrogen-Bond Network Promotes Water Splitting on the TiO2 Surface. *J. Am. Chem. Soc.* **2022**, *144*, 13565−13573. (c) Xin, Y.; Wang, S.; Yuan, H.; Hou, T.; Zhu, W.; Liu, Y.; Yao, Y.; Zhang, W.; Liang, S.; Wang, L. Atomic-level insights into the activation of nitrogen via hydrogen-bond interaction toward nitrogen photofixation. *Chem.* **2021**, *7*, 2118−2136. (d) Yue, J.; Li, Y.; Yang, C.; Luo, W. Hydroxyl-Binding Induced Hydrogen Bond Network Connectivity on Ru-based Catalysts for Efficient Alkaline Hydrogen Oxidation Electrocatalysis. *Angew. Chem., Int. Ed.* **2025**, *64*, No. e202415447.
(23) Sankar, M.; Nowicka, E.; Tiruvalam, R.; He, Q.; Taylor, S. H.; Kiely, C. J.; Bethell, D.; Knight, D. W.; Hutchings, G. J. Controlling the duality of the mechanism in liquid-phase oxidation of benzyl alcohol catalysed by supported Au-Pd nanoparticles. *Chemistry* **2011**, *17*, 6524−6532.
(24) Lin, X. X.; Zhang, X. F.; Wang, A. J.; Fang, K. M.; Yuan, J.; Feng, J. J. Simple one-pot aqueous synthesis of AuPd alloy nanocrystals/reduced graphene oxide as highly efficient and stable electrocatalyst for oxygen reduction and hydrogen evolution reactions. *J. Colloid Interface Sci.* **2017**, *499*, 128−137.
(25) He, L.-L.; Song, P.; Feng, J.-J.; Huang, W.-H.; Wang, Q.-L.; Wang, A.-J. Simple wet-chemical synthesis of alloyed PdAu nanochain networks with improved electrocatalytic properties. *Electrochim. Acta* **2015**, *176*, 86−95.
(26) Lim, J.-S.; Kim, S.-M.; Lee, S.-Y.; Stach, E. A.; Culver, J. N.; Harris, M. T. Formation of Au/Pd Alloy Nanoparticles on TMV. *J. Nanomater.* **2010**, *2010*, No. 620505.
(27) (a) Chai, J.; Li, F.; Hu, Y.; Zhang, Q.; Han, D.; Niu, L. Hollow flower-like AuPd alloy nanoparticles: One step synthesis, self-assembly on ionic liquid-functionalized graphene, and electro-oxidation of formic acid. *J. Mater. Chem.* **2011**, *21*, 17922−17929. (b) Xu, J.; White, T.; Li, P.; He, C.; Yu, J.; Yuan, W.; Han, Y. F. Biphasic Pd-Au alloy catalyst for low-temperature CO oxidation. *J. Am. Chem. Soc.* **2010**, *132*, 10398−10406. (c) Nascente, P. A.; de Castro, S. G.; Landers, R.; Kleiman, G. G. X-ray photoemission and Auger energy shifts in some gold-palladium alloys. *Phys. Rev. B Condens Matter* **1991**, *43*, 4659−4666. (d) Kim, S.; Park, S.; Park, S.; Lee, C. Acetone sensing of Au and Pd-decorated WO3 nanorod sensors. *Sens. Actuators, B* **2015**, *209*, 180−185.
(28) Guo, K. Poly(acrylonitrile) encapsulated graphite as anode materials for lithium ion batteries. *J. Power Sources* **2002**, *111*, 350−356.
(29) Zhang, Y.; Wang, F.; Pan, L.; Wang, B.; Li, Y. Facile Synthesis of High-Molecular-Weight Vinyl Sulfone (Sulfoxide) Modified Polyethylenes via Coordination−Insertion Copolymerization. *Macromolecules* **2020**, *53*, 5177−5187.
(30) (a) Kuwahara, Y.; Kango, H.; Yamashita, H. Catalytic Transfer Hydrogenation of Biomass-Derived Levulinic Acid and Its Esters to γ-Valerolactone over Sulfonic Acid-Functionalized UiO-66. *ACS Sustainable Chem. Eng.* **2017**, *5*, 1141−1152. (b) Oh, K. I.; Rajesh, K.; Stanton, J. F.; Baiz, C. R. Quantifying Hydrogen-Bond Populations in Dimethyl Sulfoxide/Water Mixtures. *Angew. Chem., Int. Ed. Engl.* **2017**, *56*, 11375−11379. (c) Issidorides, C. H.; Haddadin, M. J. Benzofurazan oxide. II. Reactions with enolate anions. *Journal of Organic Chemistry* **1966**, *31*, 4067−4068.
(31) (a) Liu, X.; Luo, Y.; Ma, H.; Zhang, S.; Che, P.; Zhang, M.; Gao, J.; Xu, J. Hydrogen-Binding-Initiated Activation of O-H Bonds on a Nitrogen-Doped Surface for the Catalytic Oxidation of Biomass Hydroxyl Compounds. *Angew. Chem., Int. Ed. Engl.* **2021**, *60*, 18103−18110. (b) Luo, Y.; Ma, H.; Sun, Y.; Che, P.; Nie, X.; Wang, T.; Xu, J. Understanding and Measurement for the Binding Energy of Hydrogen bonds of Biomass-Derived Hydroxyl Compounds. *J. Phys. Chem. A* **2018**, *122*, 843−848.
(32) (a) Xie, D.; Pu, Y.; Meng, X.; Bryant, N. D.; Zhang, K.; Wang, W.; Ragauskas, A. J.; Li, M. Effect of the Lignin Structure on the Physicochemical Properties of Lignin-Grafted-Poly(ε-caprolactone) and Its Application for Water/Oil Separation. *ACS Sustainable Chem. Eng.* **2022**, *10*, 16882−16895. (b) Manayil, J. C.; dos Santos, V. C.; Jentoft, F. C.; Granollers Mesa, M.; Lee, A. F.; Wilson, K. Octyl Co-

https://doi.org/10.1021/jacsau.4c01262
JACS Au 2025, 5, 1359−1366

grafted PrSO3H/SBA-15: Tunable Hydrophobic Solid Acid Catalysts for Acetic Acid Esterification. *ChemCatChem.* **2017**, *9*, 2231−2238. (c) Ojah, N.; Saikia, D.; Gogoi, D.; Baishya, P.; Ahmed, G. A.; Ramteke, A.; Choudhury, A. J. Surface modification of core-shell silk/PVA nanofibers by oxygen dielectric barrier discharge plasma: Studies of physico-chemical properties and drug release behavior. *Appl. Surf. Sci.* **2019**, *475*, 219−229.

(33) Dierks, M.; Cao, Z.; Manayil, J. C.; Akilavasan, J.; Wilson, K.; Schüth, F.; Rinaldi, R. Impact of Hydrophobic Organohybrid Silicas on the Stability of Ni2P Catalyst Phase in the Hydrodeoxygenation of Biophenols. *ChemCatChem.* **2018**, *10*, 2219−2231.

(34) Hasegawa, S.; Masuda, S.; Takano, S.; Harano, K.; Kikkawa, J.; Tsukuda, T. Synergistically Activated Pd Atom in Polymer-Stabilized Au(23)Pd(1) Cluster. *ACS Nano* **2022**, *16*, 16932−16940.

(35) (a) Kari, J.; Olsen, J. P.; Jensen, K.; Badino, S. F.; Krogh, K. B. R. M.; Borch, K.; Westh, P. Sabatier Principle for Interfacial (Heterogeneous) Enzyme Catalysis. *ACS Catal.* **2018**, *8*, 11966−11972. (b) Sabatier, P. Hydrogénations et déshydrogénations par catalyse. *Berichte der deutschen chemischen Gesellschaft* **1911**, *44*, 1984−2001. (c) Kuo, D. Y.; Kawasaki, J. K.; Nelson, J. N.; Kloppenburg, J.; Hautier, G.; Shen, K. M.; Schlom, D. G.; Suntivich, J. Influence of Surface Adsorption on the Oxygen Evolution Reaction on IrO(2)(110). *J. Am. Chem. Soc.* **2017**, *139*, 3473−3479. (d) Arnling Baath, J.; Jensen, K.; Borch, K.; Westh, P.; Kari, J. Sabatier Principle for Rationalizing Enzymatic Hydrolysis of a Synthetic Polyester. *JACS Au* **2022**, *2*, 1223−1231.

https://doi.org/10.1021/jacsau.4c01262
JACS Au 2025, 5, 1359−1366